

Octupole correlations of the $K^{\pi}=5/2^{+}$ ground-state band in ^{229}Th

Yuan-Yuan Wang(王媛媛) and Peng-Wei Zhao(赵鹏巍)

Citation: Chin. Phys. B, 2026, 35 (**2**): 020603. DOI: 10.1088/1674-1056/ae13ee
http://cpb.iphy.ac.cn; http://iopscience.iop.org/cpb

What follows is a list of articles you may be interested in

Progresses on Th-doped materials for solid-state nuclear clock

Cheng-Chun Zhao(赵呈春), Lin Li(李琳), Shan-Ming Li(李善明), Qiao-Rui Gong(龚巧瑞), Pei-Xiong Zhang(张沛雄), Yin Hang(杭寅), Long-Sheng Ma(马龙生), and Shi-Ning Zhu(祝世宁)

Chin. Phys. B, 2026, 35 (**2**): 020602. DOI: 10.1088/1674-1056/ae210f

Progresses on 148 nm light sources for precision measurement of nuclear transition of ^{229m}Th

Yang Wang(王样), Zheng-Rong Xiao(肖峥嵘), Heng-Zhi Zhang(张恒之), Lin-Qiang Hua(华林强), and Xiao-Jun Liu(柳晓军)

Chin. Phys. B, 2026, 35 (**2**): 020601. DOI: 10.1088/1674-1056/ae0d78

Enhanced timing of a 113 km O-TWTFT link with complex maximum likelihood estimation process

Yu-Chen Fang(方宇辰), Jian-Yu Guan(管建宇), Qi Shen(沈奇), Jin-Jian Han(韩金剑), Lei Hou(侯磊), Meng-Zhe Lian(连蒙浙), Yong Wang(王勇), Wei-Yue Liu(刘蔚悦), Ji-Gang Ren(任继刚), Cheng-Zhi Peng(彭承志), Qiang Zhang(张强), Hai-Feng Jiang(姜海峰), and Jian-Wei Pan(潘建伟)

Chin. Phys. B, 2026, 35 (**1**): 010602. DOI: 10.1088/1674-1056/ae1120

Phasemeter based on second harmonic signal filter for space-based gravitational wave detection

Zheng Fan(范正), Zhu Li(李祝), Xiangqing Huang(黄祥青), Yurong Liang(梁浴榕), Yu Song(宋煜), Maomao Fan(范毛毛), Huizong Duan(段会宗), Siyuan Peng(彭思远), Shanqing Yang(杨山清), and Liangcheng Tu(涂良成)

Chin. Phys. B, 2026, 35 (**1**): 010601. DOI: 10.1088/1674-1056/ae1efe

Finite time hybrid synchronization of heterogeneous duplex complex networks via time-varying intermittent control

Cheng-Jun Xie(解成俊) and Xiang-Qing Lu(卢向清)

Chin. Phys. B, 2025, 34 (**4**): 040601. DOI: 10.1088/1674-1056/adacc6

SPECIAL TOPIC — Advances in thorium nuclear optical clocks

Octupole correlations of the $K^\pi = 5/2^+$ ground-state band in ^{229}Th

Yuan-Yuan Wang(王媛媛)[1] and Peng-Wei Zhao(赵鹏巍)[2,†]

[1] *Mathematics and Physics Department, North China Electric Power University, Beijing* 102206, *China*
[2] *State Key Laboratory of Nuclear Physics and Technology, School of Physics, Peking University, Beijing* 100871, *China*

(Received 13 August 2025; revised manuscript received 3 October 2025; accepted manuscript online 16 October 2025)

The octupole correlations of the $K^\pi = 5/2^+$ ground state and the rotational spectrum built on it in ^{229}Th are studied using the microscopic relativistic density functional theory on a three-dimensional lattice space and the reflection-asymmetric triaxial particle rotor model. It is found that ^{229}Th has a ground state with static axial octupole and quadrupole deformations. The occurrence of octupole correlations, driven by the octupole deformation, is analyzed through the evolution of single-particle levels around the Fermi surface. The experimental energy spectrum and the electromagnetic transition probabilities, including $B(E2)$ and $B(M1)$, are reasonably well reproduced.

Keywords: octupole correlation, relativistic density functional theory, reflection-asymmetric triaxial particle rotor model, rotational spectrum

PACS: 06.30.Ft, 21.10.–k, 21.60.–n, 21.60.Jz, 23.20.–g

DOI: 10.1088/1674-1056/ae13ee **CSTR:** 32038.14.CPB.ae13ee

1. Introduction

The atomic nucleus ^{229}Th has garnered sustained attention not only in nuclear physics but also in atomic physics, laser physics, and metrology, owing to the presence of an extremely low-energy (~ 8 eV) $K^\pi = 3/2^+$ isomeric state.[1–8] This extraordinary low-energy isomeric state is the most promising candidate known so far for developing a nuclear clock utilizing current laser technology.[9–12] Such a nuclear clock would enable a variety of applications, including dark matter research,[11,13,14] relativistic geodesy,[15] and the observation of potential temporal variations of fundamental constants,[11,16,17] see e.g., reviews.[18,19]

From a nuclear structure perspective, the actinide isotope ^{229}Th serves as a paradigmatic example of heavy nuclei, featuring pronounced collectivity and the possibility of octupole (reflection-asymmetric) deformation.[20,21] The excited level structure of ^{229}Th has been extensively studied experimentally via α decay of ^{233}U,[22–25] β decay of ^{229}Ac,[26,27] Coulomb excitations,[28] and ^{230}Th$(d,t)^{229}$Th reactions.[29] Focusing on the level structure built on the $K^\pi = 5/2^+$ ground state and the $K^\pi = 3/2^+$ isomeric state, the corresponding collective rotational bands were reported by Kroger and Reich half a century ago.[22] They classified these two bands, built on the $5/2^+[633]$ and $3/2^+[631]$ Nilsson states (labeled by the Nilsson asymptotic quantum numbers), respectively. The octupole-correlated parity partner bands, i.e., the $K^\pi = 5/2^-$ partner of the ground-state band and the $K^\pi = 3/2^-$ partner of the isomeric-state band, were also identified, indicating the presence of octupole correlations in ^{229}Th.[26,27]

Theoretically, studies on the band structure of ^{229}Th have been conducted using the reflection-asymmetric particle rotor model (PRM),[30,31] the quasiparticle-plus-phonon model (QPPM),[26,27] and the coherent quadrupole-octupole model combined with the deformed shell model (CQOM+DSM),[32–34] among others. The reflection-asymmetric PRM[30,31] and QPPM[26,27] provide an overall description of the ^{229}Th spectrum without specifically addressing the isomer properties. CQOM+DSM[32–34] calculations have been performed to investigate the band structure and the formation mechanism of the isomeric state. However, none of these three theoretical approaches has explored the origin of octupole correlations in this nucleus. A unified description of the energy spectra, electromagnetic transitions, and octupole correlations of the two rotational bands based on the $K^\pi = 5/2^+$ ground state and the $K^\pi = 3/2^+$ isomeric state is needed. Such a description would aid in understanding the formation mechanism of the isomeric state and the influence of octupole correlations on it. Considering that predicting the isomer energy at the eV level remains extremely challenging from the perspective of nuclear structure theory, we initiate a preliminary investigation focusing on the $K^\pi = 5/2^+$ ground-state band. The band structure, including the energy spectrum, electromagnetic transitions, and octupole correlations, will be studied using microscopic density functional theory in combination with the quantum particle rotor model.

Starting from a universal energy density functional, nuclear density functional theory (DFT) can self-consistently describe almost all nuclei across the nuclear chart.[35,36] In re-

†Corresponding author. E-mail: pwzhao@pku.edu.cn

© 2026 Chinese Physical Society and IOP Publishing Ltd. All rights, including for text and data mining, AI training, and similar technologies, are reserved.

cent decades, relativistic DFT (RDFT) has undergone significant development and has been extensively applied to a wide range of nuclear phenomena.[35,37–39] The version of RDFT on a three-dimensional (3D) lattice space was developed[40–42] after overcoming the variational collapse[43] and Fermion doubling problems.[40,41] Recently, a preconditioned conjugate gradient method with a filtering function has been proposed to more effectively solve the nuclear Dirac equation under a given potential in 3D lattice space.[44,45] To date, RDFT on a 3D lattice has served as a powerful tool for exploring exotic nuclear shapes and their excitation modes, including nuclear linear chains,[42,46] chiral rotation,[47] toroidal structures,[48] octupole shapes,[45,49,50] and rotational properties of transfermium nuclei,[51] among others. Since no spatial symmetry restrictions are imposed on the single-particle wave functions, RDFT on a 3D lattice provides an appropriate framework to investigate the occurrence of octupole correlations in ^{229}Th. In this work, RDFT is solved on a 3D lattice and applied to explore the octupole correlation of the $K^\pi = 5/2^+$ ground state in ^{229}Th within a full deformation space.

To further investigate the rotational spectrum built on the $K^\pi = 5/2^+$ ground state, the reflection-asymmetric triaxial particle rotor model (RAT-PRM)[52] including both octupole and triaxial degrees of freedom is also employed. This model was first developed in Ref. [52] to investigate octupole correlations between chiral doublet bands.[52–54] By analyzing the RAT-PRM Hamiltonian, a new symmetry for an ideal chirality-parity violation system was identified, and the corresponding selection rules for electromagnetic transitions were derived.[55] Furthermore, RAT-PRM has been widely used to study the rotational spectra and electromagnetic properties of possible parity-doublet bands across different mass regions.[56–62]

In this paper, RDFT on a 3D lattice and RAT-PRM are employed to study the octupole correlations of the $K^\pi = 5/2^+$ ground state and the rotational spectrum built on it in ^{229}Th. The models are briefly introduced in Section 2. The calculated results and numerical details are discussed in Section 3, and a summary is presented in Section 4.

2. Theoretical framework

2.1. Formalism of the RDFT

The RDFT framework starts from a standard point-coupling Lagrangian density, which is given by[63]

$$\begin{aligned}\mathcal{L} &= \mathcal{L}^{\text{free}} + \mathcal{L}^{\text{4f}} + \mathcal{L}^{\text{hot}} + \mathcal{L}^{\text{der}} + \mathcal{L}^{\text{em}} \\ &= \bar{\psi}(\mathrm{i}\gamma_\mu\partial^\mu - m)\psi - \frac{1}{2}\alpha_{\text{S}}(\bar{\psi}\psi)(\bar{\psi}\psi) \\ &\quad -\frac{1}{2}\alpha_{\text{V}}(\bar{\psi}\gamma_\mu\psi)(\bar{\psi}\gamma^\mu\psi) \\ &\quad -\frac{1}{2}\alpha_{\text{TS}}(\bar{\psi}\boldsymbol{\tau}\psi)(\bar{\psi}\boldsymbol{\tau}\psi) - \frac{1}{2}\alpha_{\text{TV}}(\bar{\psi}\boldsymbol{\tau}\gamma_\mu\psi)(\bar{\psi}\boldsymbol{\tau}\gamma^\mu\psi) \\ &\quad -\frac{1}{3}\beta_{\text{S}}(\bar{\psi}\psi)^3 - \frac{1}{4}\gamma_{\text{S}}(\bar{\psi}\psi)^4 - \frac{1}{4}\gamma_{\text{V}}[(\bar{\psi}\gamma_\mu\psi)(\bar{\psi}\gamma^\mu\psi)]^2 \\ &\quad -\frac{1}{2}\delta_{\text{S}}\partial_\nu(\bar{\psi}\psi)\partial^\nu(\bar{\psi}\psi) - \frac{1}{2}\delta_{\text{V}}\partial_\nu(\bar{\psi}\gamma_\mu\psi)\partial^\nu(\bar{\psi}\gamma^\mu\psi) \\ &\quad -\frac{1}{2}\delta_{\text{TS}}\partial_\nu(\bar{\psi}\boldsymbol{\tau}\psi)\partial^\nu(\bar{\psi}\boldsymbol{\tau}\psi) \\ &\quad -\frac{1}{2}\delta_{\text{TV}}\partial_\nu(\bar{\psi}\boldsymbol{\tau}\gamma_\mu\psi)\partial^\nu(\bar{\psi}\boldsymbol{\tau}\gamma_\mu\psi) \\ &\quad -\frac{1}{4}F^{\mu\nu}F_{\mu\nu} - e\frac{1-\tau_3}{2}\bar{\psi}\gamma^\mu\psi A_\mu, \end{aligned} \tag{1}$$

where m denotes the nucleon mass and e the proton charge unit. $F_{\mu\nu}$ is the electromagnetic field strength tensor, while A_μ is the four-vector potential. α_{S}, α_{V}, α_{TS}, α_{TV}, β_{S}, γ_{S}, γ_{V}, δ_{S}, δ_{V}, δ_{TS}, and δ_{TV} are the eleven coupling constants, where α denotes four-fermion terms, β and γ refer to third- and fourth-order terms, respectively, and δ represents derivative couplings. S, V, and T correspond to scalar, vector, and isovector couplings, respectively.

According to the variational principle, the Dirac equation for nucleons can be derived

$$\begin{aligned}&\hat{h}(\boldsymbol{r})\psi_k(\boldsymbol{r}) \\ &= [\boldsymbol{\alpha}\cdot(-\mathrm{i}\boldsymbol{\nabla} - V(\boldsymbol{r})) + \beta(m + S(\boldsymbol{r})) + V^0(\boldsymbol{r})]\psi_k(\boldsymbol{r}) \\ &= \varepsilon_k\psi_k(\boldsymbol{r}), \end{aligned} \tag{2}$$

where ε_k represents the single-particle energy. The relativistic vector field $V_\mu(\boldsymbol{r})$ and scalar $S(\boldsymbol{r})$ are self-consistently connected to the nucleon densities and currents. The single-particle energies, along with expectation values of angular momentum, quadrupole, and octupole moments, can be obtained by solving the Dirac equation (2) on a 3D lattice space self-consistently, as detailed in Refs. [41,42,44,45].

2.2. Formalism of the RAT-PRM

The detailed RAT-PRM formalism is outlined in Ref. [52]. The total Hamiltonian is the sum of the intrinsic Hamiltonian $\hat{H}^{\text{p(n)}}_{\text{intr.}}$ for valence protons (neutrons) and the collective Hamiltonian $\hat{H}_{\text{core}}$ of a reflection-asymmetric triaxial rotor.

The intrinsic Hamiltonian $\hat{H}^{\text{n}}_{\text{intr.}}$ for valence neutrons reads[64–66]

$$\begin{aligned}\hat{H}^{\text{n}}_{\text{intr.}} &= \sum_{\nu>0}(\varepsilon^{\text{n}}_\nu - \lambda_n)(a^\dagger_\nu a_\nu + a^\dagger_{\bar{\nu}}a_{\bar{\nu}}) \\ &\quad -\frac{\Delta}{2}\sum_{\nu>0}(a^\dagger_\nu a^\dagger_{\bar{\nu}} + a_{\bar{\nu}}a_\nu), \end{aligned} \tag{3}$$

where Δ is the pairing gap parameter and λ_n is the Fermi energy. To obtain the single-neutron energy $\varepsilon^{\text{n}}_\nu$, one diagonalizes the reflection-asymmetric triaxial single-particle Hamiltonian with a Nilsson form $\hat{H}^{\text{n}}_{\text{s.p.}}$ [52,67]

$$\hat{H}^{\text{n}}_{\text{s.p.}} = -\frac{1}{2}\hbar\omega_0\nabla^2 + V(r;\theta,\varphi) + C\boldsymbol{l}\cdot\boldsymbol{s} + D[\boldsymbol{l}^2 - \langle\boldsymbol{l}^2\rangle_N], \tag{4}$$

where the terms correspond to the kinetic energy, reflection-asymmetric triaxially deformed potential,[52] spin–orbit, and

the shifting term. $C = -2\kappa$ and $D = -\kappa\mu$ are parameters related to the standard Nilsson parameters κ and μ.

The core Hamiltonian $\hat{H}_{\rm core}$ reads

$$\hat{H}_{\rm core} = \sum_{k=1}^{3} \frac{\hat{R}_k^2}{2\mathcal{J}_k} + \frac{1}{2}E(0^-)(1-\hat{P}_{\rm c}), \tag{5}$$

where $\hat{R}_k$ and $\hat{P}_{\rm c}$ denote the angular momentum and parity of the core, respectively. $\mathcal{J}_k = \mathcal{J}_0 \sin^2(\gamma - 2k\pi/3)$ are the moments of inertia of irrotational-flow type, and $E(0^-)$ parametrizes the core parity splitting.

Diagonalization of the total Hamiltonian $\hat{H}$ yields eigenvalues and eigenfunctions, from which reduced electromagnetic transition probabilities can be calculated.[52]

3. Results and discussion

In the RDFT calculation, we employ the density functional PC-PK1,[63] which has been successful in previous studies. The single-particle Dirac equation (2) is represented on a 3D lattice space. We adopt a box size of 30 fm along the x, y, and z axes with a step size of 1 fm. The iteration is considered converged if the following criteria are met: the absolute difference between the mean potentials of two consecutive iterations is no more than 10^{-3} MeV, and the uncertainty of energy for each occupied single-particle state, $\langle\hat{h}^2\rangle_i - \langle\hat{h}\rangle_i^2$, is less than 10^{-9} MeV^2. We performed a deformation-constrained RDFT calculation on a 3D lattice for $\beta_{20} \in [0, 0.35]$ and $\beta_{30} \in [0, 0.3]$ with a step size of 0.05 to obtain the potential energy surface (PES) in the (β_{20}, β_{30}) plane.

Figure 1 shows the calculated PES in the (β_{20}, β_{30}) plane for ^{229}Th using RDFT on a 3D lattice with PC-PK1.[63] The global minimum of the PES is located at $\beta_{20} = 0.23$ and $\beta_{30} = 0.15$. No symmetry restrictions are imposed on the single-particle wave functions in RDFT, and all deformation degrees of freedom are included self-consistently. In addition to the constrained axial quadrupole deformation β_{20} and octupole deformation β_{30}, the axial hexadecapole deformation $\beta_{40} = 0.18$ is obtained self-consistently for the ground state of ^{229}Th. All axial asymmetric deformations, i.e., $\beta_{2\mu}, \beta_{3\mu}, \beta_{4\mu}$ with $\mu \neq 0$, are found to be zero, indicating that the ground state assumes an axially symmetric and reflection-asymmetric shape. Furthermore, the PES is relatively soft along the octupole deformation β_{30} near the minimum. The energy difference between the lowest reflection-symmetric configuration ($\beta_{20} = 0.25$, $\beta_{30} = 0.0$) and the ground state ($\beta_{20} = 0.23$, $\beta_{30} = 0.15$) is less than 1.25 MeV. Pairing correlations are neglected in the present RDFT calculation; their inclusion modifies the ground-state deformation slightly from ($\beta_{20} = 0.23$, $\beta_{30} = 0.15$) to ($\beta_{20} = 0.22$, $\beta_{30} = 0.16$).

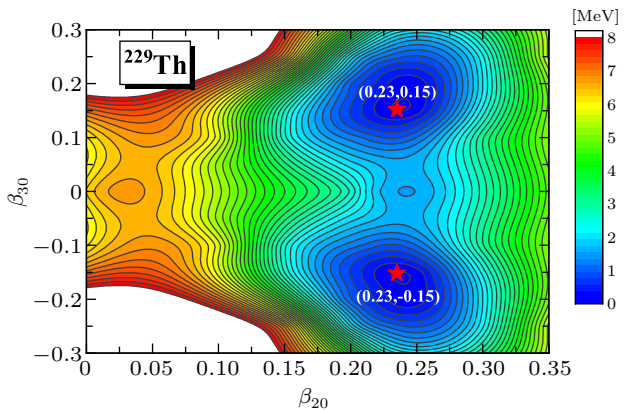


Fig. 1. Potential energy surface of ^{229}Th calculated using RDFT on a 3D lattice[41,42,44,45] with the density functional PC-PK1.[63] The energies are normalized to the ground-state energy, and the contour interval is 0.20 MeV. The pentagram indicates the location of the global minimum.

For a microscopic understanding of the emergence of octupole correlations in ^{229}Th, the calculated single-particle levels near the Fermi surface are shown in Fig. 2 as a function of the octupole deformation β_{30}. As depicted in Fig. 2(a) for the single-proton levels, an energy gap at $Z = 88$, formed by several levels near the Fermi surface, persists with increasing β_{30}. Similarly, for the single-neutron levels shown in Fig. 2(b), an energy gap at $N = 134$ exists when β_{30} is small, but this gap narrows as the octupole deformation increases, while a new gap emerges at $N = 138$ near the Fermi surface. In the $Z \approx 88$, $N \approx 134$ region, the octupole deformation of ^{229}Th empirically originates from the $\pi(\mathrm{f}_{7/2} \leftrightarrow \mathrm{i}_{13/2})$ and $\nu(\mathrm{g}_{9/2} \leftrightarrow \mathrm{j}_{15/2})$ couplings.[20,21] As shown in Figs. 2(a) and 2(b), the last two paired protons occupy the $\mathrm{f}_{7/2}$ orbitals, while the valence neutron occupies the $\mathrm{g}_{9/2}$ orbital. The coupling between the proton $\mathrm{f}_{7/2}$ and $\mathrm{i}_{13/2}$ orbitals, as well as between the neutron $\mathrm{g}_{9/2}$ and $\mathrm{j}_{15/2}$ orbitals, leads to the emergence of octupole correlations in ^{229}Th.

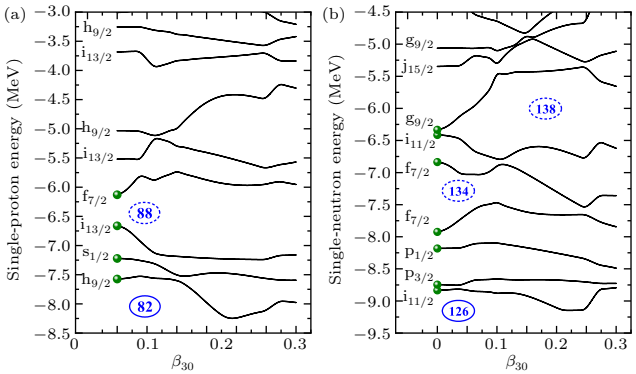


Fig. 2. Single-particle levels of ^{229}Th for (a) protons and (b) neutrons as functions of the octupole deformation β_{30}. Each level is labeled by the spherical quantum number of its dominant component.

With the above information on the deformation and configuration of the ground state of ^{229}Th, the rotational spectrum based on the ground state is investigated using the RAT-PRM. In the RAT-PRM calculation, the deformation parameters $\beta_{20} = 0.23$ and $\beta_{30} = 0.15$ are adopted from the global

minimum of the PES calculated by RDFT (Fig. 1). For the intrinsic part, the valence neutron space is spanned by three j-orbitals, including a high-j intruder negative-parity orbital $j_{15/2}$ and two positive-parity orbitals $g_{9/2}$ and $i_{11/2}$. The neutron Fermi energy $\lambda_n = 49.29$ MeV is chosen corresponding to the parity-mixed orbital $\nu(g_{9/2},j_{15/2})$, and the pairing gap takes the empirical form $\Delta = 12/\sqrt{A}$ MeV.[68] For the collective core, the core parity splitting parameter $E(0^-) = 0$ MeV and the moment of inertia $\mathcal{J}_0 = 74\hbar^2$ MeV^{-1} are adopted to reproduce the experimental energy spectra. In PRM descriptions, an *ad hoc* Coriolis attenuation factor ξ is generally introduced,[69,70] and its value is set to 0.4 in the present calculation to reproduce the signature splitting of the experimental spectra. For the calculation of electromagnetic transition properties, the intrinsic electric-quadrupole moment $Q_0 = (3/\sqrt{5\pi})R_0^2 Z\beta_{20}$ with $R_0 = 1.2A^{1/3}$ fm, and the effective gyromagnetic factor for the collective core $g_R = Z/A \approx 0.393$ are adopted.[68] The gyromagnetic factor of the valence neutron, $g_n = -0.062$, is adjusted to reproduce the experimental magnetic moment of the ground state.

The calculated energy spectra of the $K^\pi = 5/2^+$ ground-state band in ^{229}Th are shown in Fig. 3, together with the corresponding experimental spectra.[71] The RAT-PRM calculation reproduces the experimental energy spectra reasonably well. The configuration of the $K^\pi = 5/2^+$ ground-state band is dominated by $\nu g_{9/2}[\Omega = 5/2]$, corresponding to the $5/2[633]$ Nilsson orbital mixed with the $j_{15/2}[\Omega = 5/2]$ orbital due to octupole correlations. To investigate the effect of octupole deformation, a RAT-PRM calculation with $\beta_{30} = 0.00$ was also performed, which shows that the excitation energies are largely insensitive to the change of β_{30} from 0.15 to 0.00, except for variations of several to over a dozen keV.

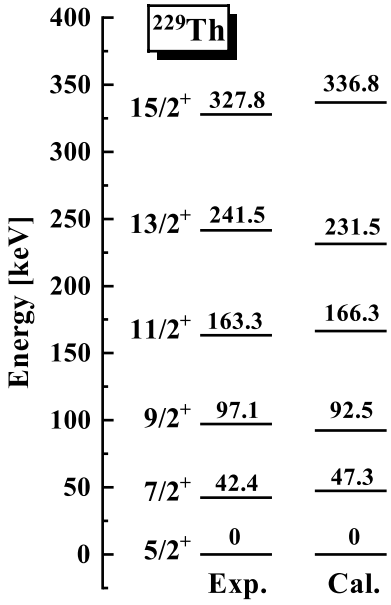


Fig. 3. Calculated energies of the $K^\pi = 5/2^+$ ground-state band in ^{229}Th using RAT-PRM, compared with available experimental data.[71]

Table 1. Calculated $E2$ and $M1$ transition probabilities for the low-lying $K^\pi = 5/2^+$ ground-state band of ^{229}Th, compared with available experimental data.[72]

Type	Transition	Exp.(Err) (W.u.)	Cal. (W.u.)
$E2$	$\frac{7^+}{2}_{yr} \to \frac{5^+}{2}_{yr}$	300(±16)	192
$E2$	$\frac{9^+}{2}_{yr} \to \frac{5^+}{2}_{yr}$	65(±7)	83
$E2$	$\frac{9^+}{2}_{yr} \to \frac{7^+}{2}_{yr}$	170(±30)	133
$M1$	$\frac{7^+}{2}_{yr} \to \frac{5^+}{2}_{yr}$	0.0110 (±0.0040)	0.0064
$M1$	$\frac{9^+}{2}_{yr} \to \frac{7^+}{2}_{yr}$	0.0076 (±0.0012)	0.0553

Table 1 presents the calculated intraband $\Delta I = 1\hbar$ and $\Delta I = 2\hbar$ $B(E2)$ values, as well as the $B(M1)$ values, compared with available experimental data.[72] For the $E2$ transitions, the present RAT-PRM results reproduce both the $\Delta I = 1\hbar$ and $\Delta I = 2\hbar$ $B(E2)$ data well. Specifically, the $\Delta I = 1\hbar$ transitions are slightly underestimated, whereas the $\Delta I = 2\hbar$ transitions are slightly overestimated. As shown in Table 1, while the calculated $B(E2)$ values generally agree with the experimental data, the calculated $B(M1)$ values differ from the experimental ones by nearly an order of magnitude. Given that $B(E2)$ reflects the collective behavior of the nucleus, whereas $B(M1)$ is more sensitive to single-particle properties, the present level of agreement for $B(M1)$ is considered reasonably satisfactory.

4. Conclusion

In summary, the $K^\pi = 5/2^+$ ground-state band of ^{229}Th has been investigated using microscopic RDFT on a 3D lattice combined with the RAT-PRM. The constrained RDFT calculation on a 3D lattice yields the potential energy surface in the (β_{20},β_{30}) plane, indicating a static axial quadrupole and octupole deformed ground state. Driven by the octupole deformation β_{30}, the evolution of single-particle levels near the Fermi surface is analyzed, revealing the origin of octupole correlations, which can be attributed to the coupling of neutron $g_{9/2}$ and $j_{15/2}$ orbitals and proton $f_{7/2}$ and $i_{13/2}$ orbitals. Based on the deformation parameters and configuration obtained from RDFT, the energy spectra, $B(E2)$, and $B(M1)$ values are calculated with RAT-PRM, reproducing the available experimental data for the $K^\pi = 5/2^+$ ground-state band.

The present description of the $K^\pi = 5/2^+$ band provides a solid basis for further studies. Future work will extend the RDFT + RAT-PRM framework to the $K^\pi = 3/2^+$ isomeric band, including its energy spectrum (especially the isomer energy), and both intraband and interband electromagnetic transitions.

Acknowledgments

This work is supported by the National Natural Science Foundation of China (Grant Nos. 12205097, 12141501, 12475117, and 12435006), the National Key Laboratory of Neutron Science and Technology (Grant No. NST202401016), the National Key R&D Program of China (Grant Nos. 2024YFA1612600 and 2024YFE0109803), and the High-performance Computing Platform of Peking University.

References

[1] Beck B R, Becker J A, Beiersdorfer P, Brown G V, Moody K J, Wilhelmy J B, Porter F S, Kilbourne C A and Kelley R L 2007 *Phys. Rev. Lett.* **98** 142501
[2] Seiferle B, Wense L von der, Bilous P V, Amersdorffer I, Lemell C, Libisch F, Stellmer S, Schumm T, Düllmann C E, Pálffy A and Thirolf P G 2019 *Nature* **573** 243
[3] Yamaguchi A, Muramatsu H, Hayashi T, Yuasa N, Nakamura K, Takimoto M, Haba H, Konashi K, Watanabe M, Kikunaga H, Maehata K, Yamasaki N Y and Mitsuda K 2019 *Phys. Rev. Lett.* **123** 222501
[4] Sikorsky T, Geist J, Hengstler D, Kempf S, Gastaldo L, Enss C, Mokry C, Runke J, Düllmann C E, Wobrauschek P, Beeks K, Rosecker V, Sterba J H, Kazakov G, Schumm T and Fleischmann A 2020 *Phys. Rev. Lett.* **125** 142503
[5] Kraemer S, Moens J, Athanasakis-Kaklamanakis M, *et al.* 2023 *Nature* **617** 706
[6] Hiraki T, Okai K, Bartokos M, *et al.* 2024 *Nat. Commun.* **15** 5536
[7] Elwell R, Schneider C, Jeet J, Terhune J E S, Morgan H W T, Alexandrova A N, Tran T H B, Derevianko A and Hudson E R 2024 *Phys. Rev. Lett.* **133** 013201
[8] Tiedau J, Okhapkin M V, Zhang K, Thielking J, Zitzer G, Peik E, Schaden F, Pronebner T, Morawetz I, De Col L Toscani, Schneider F, Leitner A, Pressler M, Kazakov G A, Beeks K, Sikorsky T and Schumm T 2024 *Phys. Rev. Lett.* **132** 182501
[9] Peik E and Tamm C 2003 *Euro. Phys. Lett.* **61** 181
[10] Campbell C J, Radnaev A G, Kuzmich A, Dzuba V A, Flambaum V V and Derevianko A 2012 *Phys. Rev. Lett.* **108** 120802
[11] Peik E, Schumm T, Safronova M, Pálffy A, Weitenberg J and Thirolf P G 2021 *Quantum Sci. Technol.* **6** 034002
[12] Beeks K, Sikorsky T, Schumm T, Thielking J, Okhapkin M V and Peik E 2021 *Nat. Rev. Phys.* **3** 238
[13] Derevianko A and Pospelov M 2014 *Nat. Phys.* **10** 933
[14] Tsai Y D, Eby J and Safronova M S 2023 *Nat. Astro.* **7** 113
[15] Mehlstäubler T E, Grosche G, Lisdat C, Schmidt P O and Denker H 2018 *Rep. Prog. Phys.* **81** 064401
[16] Flambaum V V 2006 *Phys. Rev. Lett.* **97** 092502
[17] Fadeev P, Berengut J C and Flambaum V V 2020 *Phys. Rev. A* **102** 052833
[18] Wense L von der and Seiferle B 2020 *Eur. Phys. J. A* **56** 277
[19] Thirolf P G, Kraemer S, Moritz D and Scharl K 2024 *Eur. Phys. J. Spec. Top.* **233** 1113
[20] Butler P A and Nazarewicz W 1996 *Rev. Mod. Phys.* **68** 349
[21] Butler P A 2016 *J. Phys. G: Nucl. Part. Phys.* **43** 073002
[22] Kroger L A and Reich C W 1976 *Nucl. Phys. A* **259** 29
[23] Canty M J, Connor R D, Dohan D A and Pople B 1977 *J. Phys. G: Nucl. Phys.* **3** 421
[24] Reich C W and Helmer R G 1990 *Phys. Rev. Lett.* **64** 271
[25] Barci V, Ardisson G, Barci-Funel G, Weiss B, El Samad O and Sheline R K 2003 *Phys. Rev. C* **68** 034329
[26] Gulda K, Kurcewicz W, Aas A J, *et al.* 2002 *Nucl. Phys. A* **703** 45
[27] Ruchowska E, Płóciennik W A, Żylicz J, *et al.* 2006 *Phys. Rev. C* **73** 044326
[28] Bemis Jr C E, McGowan F K, Ford Jr J L C, Milner W T, Robinson R L, Stelson P H, Leander G A and Reich C W 1988 *Phys. Scr.* **38** 657
[29] Burke D G, Garrett P E, Qu T and Naumann R A 1990 *Phys. Rev. C* **42** 499
[30] Leander G A and Sheline R K 1984 *Nucl. Phys. A* **413** 375
[31] Leander G A and Chen Y S 1988 *Phys. Rev. C* **37** 2744
[32] Minkov N and Pálffy A 2017 *Phys. Rev. Lett.* **118** 212501
[33] Minkov N and Pálffy A 2019 *Phys. Rev. Lett.* **122** 162502
[34] Minkov N and Pálffy A 2021 *Phys. Rev. C* **103** 014313
[35] Meng J 2016 *Relativistic Density Functional for Nuclear Structure, International Review of Nuclear Physics.* Vol 10. (Singapore: World Scientifc)
[36] Bender M and Heenen P H 2003 *Rev. Mod. Phys.* **75** 121
[37] Ring P 1996 *Prog. Part. Nucl. Phys.* **37** 193
[38] Vretenar D, Afanasjev A V, Lalazissis G A and Ring P 2005 *Phys. Rep.* **409** 101
[39] Meng J, Toki H, Zhou S G, Zhang S Q, Long W H and Geng L S 2006 *Prog. Part. Nucl. Phys.* **57** 470
[40] Tanimura Y, Hagino K and Liang H Z 2015 *Prog. Theor. Exp. Phys.* **2015** 073D01
[41] Ren Z X, Zhang S Q and Meng J 2017 *Phys. Rev. C* **95** 024313
[42] Ren Z X, Zhang S Q, Zhao P W, Itagaki N, Maruhn J A and Meng J 2019 *Sci. China Phys. Mech. Astron.* **62** 112062
[43] Hagino K and Tanimura Y 2010 *Phys. Rev. C* **82** 057301
[44] Li B, Ren Z X and Zhao P W 2020 *Phys. Rev. C* **102** 044307
[45] Xu F F, Li B, Ren Z X and Zhao P W 2024 *Phys. Rev. C* **109** 014311
[46] Zhang D D, Ren Z X, Zhao P W, Vretenar D, Nikšić T and Meng J 2022 *Phys. Rev. C* **105** 024322
[47] Ren Z X, Zhao P W and Meng J 2022 *Phys. Rev. C* **105** L011301
[48] Ren Z X, Zhao P W, Zhang S Q and Meng J 2020 *Nucl. Phys. A* **996** 121696
[49] Xu F F, Li B, Ring P and Zhao P W 2024 *Phys. Lett. B* **856** 138893
[50] Li Z K and Wang Y Y 2024 *Nucl. Sci. Tech.* **35** 139
[51] Xu F F, Wang Y K, Wang Y P, Ring P and Zhao P W 2024 *Phys. Rev. Lett.* **133** 022501
[52] Wang Y Y, Zhang S Q, Zhao P W and Meng J 2019 *Phys. Lett. B* **792** 454
[53] Wang Y Y and Zhang S Q 2020 *Phys. Rev. C* **102** 034303
[54] Wang Y P, Wang Y Y and Meng J 2020 *Phys. Rev. C* **102** 024313
[55] Wang Y Y, Wu X H, Zhang S Q, Zhao P W and Meng J 2020 *Sci. Bull.* **65** 2001
[56] Morse C, Macchiavelli A O, Crawford H L, *et al.* 2020 *Phys. Rev. C* **102** 054328
[57] Rajbanshi S, Palit R, Raut R, Wang Y Y, Ren Z X, Meng J, Chen Q B, Ali Sajad, Pai H, Babra F S, Banik R, Bhattacharya S, Bhattacharyya S, Dey P, Malik S, Mukherjee G, Laskar Md S R, Nandi S, Santra Rajkumar, Trivedi T, Ghugre S S and Goswami A 2021 *Phys. Rev. C* **104** 064316
[58] Wang Y Y 2021 *Phys. Rev. C* **104** 014318
[59] Wang Y Y, Chen Q B and Zhang S Q 2022 *Phys. Rev. C* **105** 044316
[60] Madhu, Deo A Y, Yadav Khamosh, Sahoo Dhananjaya, Wang Y Y, Wang Y K, Meng J, Suman Saket, Tandel S K, Sharma A, Ahmed I, Katre K, Devi K, Rojeeta, Dutt S, Kumar S, Yashraj, Muralithar S and Singh R P 2023 *Phys. Rev. C* **108** 014309
[61] Wang Y Y, Peng J and Zhang S Q 2024 *Phys. Rev. C* **110** 024315
[62] Wang Y Y and Zhang S Q 2025 *Chin. Phys. C* **49** 014103
[63] Zhao P W, Li Z P, Yao J M and Meng J 2010 *Phys. Rev. C* **82** 054319
[64] Hamamoto I 1976 *Nucl. Phys. A* **271** 15
[65] Hamamoto I and Mottelson B 1983 *Phys. Lett. B* **127** 281
[66] Zhang S Q, Qi B, Wang S Y and Meng J 2007 *Phys. Rev. C* **75** 044307
[67] Nilsson S G 1955 *Dan. Mat. Fys. Medd.* **29** 16
[68] Ring P and Schuck P 2004 *The Nuclear Many-Body Problem* (Berlin: Springer)
[69] Stephens F S, Kleinheinz P, Sheline R K and Simon R S 1974 *Nucl. Phys. A* **222** 235
[70] Ward D, Macchiavelli A O, Clark R M, Cline D, Cromaz M, Deleplanque M A, Diamond R M, Fallon P, Gorgen A, Hayes A B, Lane G J, Lee I Y, Nakatsukasa T, Schmidt G, Stephens F S, Svensson C E, Teng R, Vetter K and Wu C Y 2012 *Phys. Rev. C* **86** 064319
[71] http://www.nndc.bnl.gov/ensdf/
[72] http://www.nndc.bnl.gov/nudat2/